

MSDE

Molecular Systems Design & Engineering

Accepted Manuscript

This article can be cited before page numbers have been issued, to do this please use: J. A. Simonovich, A. Wanchoo, R. A. Clark, J. Park, A. Shigemoto, B. G. Keselowsky and G. A. Hudalla, *Mol. Syst. Des. Eng.*, 2025, DOI: 10.1039/D5ME00106D.



This is an Accepted Manuscript, which has been through the Royal Society of Chemistry peer review process and has been accepted for publication.

Accepted Manuscripts are published online shortly after acceptance, before technical editing, formatting and proof reading. Using this free service, authors can make their results available to the community, in citable form, before we publish the edited article. We will replace this Accepted Manuscript with the edited and formatted Advance Article as soon as it is available.

You can find more information about Accepted Manuscripts in the [Information for Authors](#).

Please note that technical editing may introduce minor changes to the text and/or graphics, which may alter content. The journal's standard [Terms & Conditions](#) and the [Ethical guidelines](#) still apply. In no event shall the Royal Society of Chemistry be held responsible for any errors or omissions in this Accepted Manuscript or any consequences arising from the use of any information it contains.

Enzymatic stability poses a considerable challenge to translation of biotherapeutics, as changes in conformational state can disrupt catalytic activity and functionality. If protein misfolding is driven by key amino acids, mutation into a more stable residue can reduce protein instability. We present a selective cysteine to serine mutation strategy for the immunomodulatory enzyme indoleamine 2,3-dioxygenase (IDO). By targeting only the most solvent accessible cysteines of IDO, the IDO mutants shared a high degree of secondary structure similarity, which in turn preserved enzymatic activity. These mutants also improved thermal stability during warm and cold storage, while also improving its therapeutic efficacy in a mouse model of psoriasis as compared to wild-type IDO. Computational predictions allowed for pre-screening of candidate mutants, where several key metrics predicted low enzymatic function in non-selective Cys-Ser mutations, which was seen after microbial expression. Not only does our work demonstrate improvements to a promising immunotherapeutic, but it also highlights the importance of employing amino acid substitution judiciously, and choosing replacement amino acids according to similarity in structural shape.



Engineering an indoleamine 2,3-dioxygenase immunotherapy via selective cysteine-to-serine mutations

Jennifer A. Simonovich¹, Arun Wanchoo¹, Ryan A. Clark¹, Junha Park¹, Ayumi Shigemoto¹, Benjamin G. Keselowsky^{1*}, Gregory A. Hudalla^{1*}

¹J. Crayton Pruitt Family Department of Biomedical Engineering, Herbert Wertheim College of Engineering, University of Florida, Gainesville, FL 32610, USA

*Co-Corresponding Authors

Gregory A. Hudalla

Tel: (352) 273-9326; Fax: (352) 273-9221; Email Address: ghudalla@bme.ufl.edu

Address: J. Crayton Pruitt Family Department of Biomedical Engineering, PO Box 116131, Gainesville, FL 32611, USA

Benjamin G. Keselowsky

Tel: (352) 273-5878; Fax: (352) 392-9791; Email Address: bgk@ufl.edu

Address: J. Crayton Pruitt Family Department of Biomedical Engineering, PO Box 116131, Gainesville, FL 32611, USA

Abstract

Indoleamine 2,3-dioxygenase is an immunomodulatory enzyme that shows great promise when delivered exogenously as a protein therapeutic. However, IDO activity is under complex redox control, mediated in part by multiple cysteine residues within its primary sequence. We have characterized three IDO mutants in which solvent-accessible cysteine residues were mutated to chemically-similar serine residues, “IDO_{C4S4}” with C112S, C159S, C206S, and C308S mutations and “IDO_{C5S3}” with C112S, C159S, and C308S mutations based on prior reports that C206 is necessary for catalytic function, and IDO_{C0S8}, in which all cysteine residues were mutated to serines. IDO_{C0S8} was expressed in poor yield and demonstrated less than 1% activity when compared to wild-type IDO. In contrast, IDO_{C4S4} and IDO_{C5S3} demonstrated robust enzymatic activity, though IDO_{C5S3} had a slower V_{\max} than wild-type and IDO_{C4S4}. Computational predictions and experimental measurements suggested a high degree of structural similarity between the wild-type IDO and IDO_{C4S4}, with subtle perturbation of α -helical content for IDO_{C5S3}. The structure of IDO_{C0S8} was predicted to be significantly different than that of wild-type IDO. IDO_{C4S4} and IDO_{C5S3} were more stable than wild-type IDO over time at physiological, ambient, and reduced temperatures, likely due to diminished oxidation of the mutant IDO forms. Based on the increased V_{\max} and robust thermal stability of IDO_{C4S4}, we fused it to the anchoring moiety galectin 3, to evaluate its effectiveness in a mouse model of psoriasis. The IDO_{C4S4}-Galectin-3 fusion blunted the rate and severity of disease as compared to wild-type IDO-Galectin-3 fusion. When compared to historical data with Cys-Ala IDO mutants, this study highlights the importance of employing amino acid substitution according to similarity in isosteric and isostructural shape to advance IDO as an immunomodulatory therapeutic.

Introduction

Indoleamine 2,3-dioxygenase (IDO), an enzyme catabolizing tryptophan (1), is an attractive immunoregulatory therapy. For example, IDO provided via overexpression in transferred cells



can ameliorate type 1 diabetes (2,3) and psoriasis (4). mRNA delivery of IDO has shown efficacy in the treatment of T cell mediated diseases (5). Exogenously supplied IDO protein confers dendritic cell resistance to LPS stimulation (6) and is a robust anti-inflammatory (7). Yet, whether delivered as a gene or as protein, IDO enzymatic activity is under complex redox control (1,8–13). Immune cell activation in diseased tissue results in increased redox factor production, which can cause oxidative and nitrosative stress, redox signaling disruption, and molecular damage (14,15). IDO cysteine residues, of which there are eight, have been reported to contribute in part to enzymatic inactivation in high oxidant conditions (8,16,17).

Cysteine residues often pose problems in protein therapeutic development. Cysteines can undergo oxidation into disulfides (18), which can lead to protein misfolding and aggregation (19). The sulfhydryls in cysteines can also oxidize into sulfinic, sulfenic, and sulfonic acids (20), which can disrupt co-factor binding (e.g., metal ion coordination) (21) and hinder substrate binding (22). Cysteine oxidation can furthermore change protein conformation, resulting in altered if not inactivated function (23,24). Given the complex character of cysteines, it can be advantageous to remove such residues, if possible to do so without significantly perturbing protein form and function.

In the case of IDO, the role of each of its eight cysteine residues is poorly defined. IDO does not contain any disulfide bridges, and cysteines in proximity to the heme active site are not thought to be directly necessary for enzymatic activity (17,25). Chemically modifying the cysteines of IDO can lead to inhibition. Selenyl-sulfide bonds formed between cysteine and the organoselenium drug ebselen inhibit IDO by changing the conformational state and disrupting enzymatic activity (26). Later work also showed multimerization and inactivation of IDO after oxidation through the formation of protein-centered radicals, though the specific amino acid residues involved have not yet been identified (8). Mutating cysteines to alanines can also reduce enzymatic activity. In particular, IDO activity decreased by more than 50% when C85, C206, C272, and C335 were individually mutated into alanines (**Supplementary Table 1**) (27).

Mutating cysteines to alanines can result in unexpected changes to protein form and function due to the differences in their side-chain chemistry (28,29). In contrast, cysteine and serine are similar in isosteric and isostructural shape, differing only by atomic substitution of the sulfur in cysteine with oxygen in serine (30,31). Cys-Ser mutations have shown successes in engineering more stable protein therapeutics. In one instance, surface Cys-Ser mutants of galectin-1 resisted oxidative inactivation by eliminating susceptibility to covalent cross-linking, thus retaining activity in oxidative environments (32). Furthermore, Cys-Ser substitutions on the surface of IL-18 improved solubility and reduced aggregation (33). In contrast, in the copper binding proteins human ATP7B and *E. coli* CueR metalloregulator, Cys-Ser mutations were not tolerated at sites where cysteine coordinated copper ions and diminished enzymatic activity (34). Thus, judicious investigation of candidate mutation sites is necessary to balance protein biophysical properties for improved stability and function.

We investigated Cys-Ser IDO mutants to determine the impact of those mutations on enzymatic function, secondary structure, stability under different storage conditions, and therapeutic effectiveness. We limited mutations to C112, C159, C206, and C308, which are the cysteine residues predicted to be most solvent accessible (i.e., on the “surface” of the protein) based on crystal structure and *in silico* predictions. We generated two mutants – IDO_{C4S4}, where all surface cysteines were mutated into serines, and IDO_{C5S3}, where C112, C159, and C308 were mutated into serines but C206 was maintained, based on a prior report suggesting its role in



enzymatic function (27). We found that both Cys-Ser mutants generally retained IDO's enzymatic function and structure. IDO_{C4S4} was observed to be the most stable variant at reduced (4 °C) and body (37 °C) temperatures and outperformed wild-type IDO domain in the fusion protein IDO-Galectin3 (IDO-Gal3) *in vivo* in an imiquimod (IMQ)-induced psoriasis mouse model.

Experimental

IDO cysteine mutants design and production

Selective mutations of cysteines into serines were formed at sites 112, 159, 206, and 308 for IDO_{C4S4} and at 112, 159, and 308 for IDO_{C5S3}. Total mutation of cysteine to serine was formed at all sites for IDO_{C0S8}. The genes encoding these mutant IDOs were inserted into pET-28a (+) vectors between NdeI and XhoI restriction sites, and were produced by and purchased from Genscript. The plasmids were then transformed into Origami B(DE3) *E. coli* competent cells (Sigma-Aldrich) for protein expression, with successful transformation confirmed by Sanger sequencing (Genewiz). Protein expression was performed using the autoinduction method (35). Bacteria were pelleted and lysed, and IDO was purified from the lysis supernatant through a HiTrap TALON cobalt column (Cytiva) and size-exclusion chromatography (GE Life Sciences). Purity was ensured by sodium dodecyl sulfate polyacrylamide gel electrophoresis (SDS-PAGE) and Coomassie staining. Yield for IDO_{C5S3} and IDO_{C4S4} mutants was ~2.8 mg and ~2.5 mg of protein per liter of growth volume, respectively. Concentration was determined via the Pierce Bradford Protein Assay Kit (ThermoFisher), prior to use. Absorbance spectra were captured by NanoDrop ND-1000 Spectrophotometer. Wild-type IDO production was performed following the same method as above. IDO-Galectin3 (Gal3) fusion mutant were engineered through a combination of the IDO_{C4S4} mutant and our previously established production of IDO-Gal3 (7). Yield for IDO_{C4S4}-Gal3 mutant was ~3.5 mg of protein per liter of growth volume.

Enzymatic activity

Wild-type IDO_{C8S0}, IDO_{C5S3}, and IDO_{C4S4} were stored at 4 °C, room temperature, and 37 °C, and were sampled periodically to test for changes in enzymatic activity, with no additional steps taken to reduce oxidizing conditions. 17.88 pmoles of IDO was combined with tryptophan, catalase, and the electron donors methylene blue and ascorbic acid. The absorbance of N-formyl-kynurenine (NFK), a precursor to kynurenine, was read at 321 nm for ten minutes, and specific activity (unit of pmol NFK * min⁻¹ * pmol⁻¹ IDO) was determined from the slope of absorbance at 321 nm and the extinction coefficient of NFK, with a pathlength of 0.32 cm. Enzymatic activity for all timepoints were normalized against t=0 IDO activity, and activity half-life was calculated via best fit. The kinetic parameters of wild-type IDO_{C8S0}, IDO_{C5S3}, and IDO_{C4S4} were determined by the Michaelis-Menten equation after varying tryptophan concentrations. Activity half-life and IDO kinetic parameters were compared using a one-way ANOVA and Tukey's multiple comparison test (Graphpad Prism).

In silico analysis

Predicted secondary structures of wild-type IDO_{C8S0}, IDO_{C5S3}, and IDO_{C4S4} were generated using AlphaFold v3 (36). Structural similarity was assessed by rigid FATCAT pairwise structural alignment(37,38) (PDB) comparison of root mean square deviation of atomic positions (RMSD) and template modeling (TM) score. Predicted secondary structure composition for each protein was calculated using STRIDE (39), and then percentage of each structural component was



compared between wild-type IDO_{C8S0} vs IDO_{C5S3} and IDO_{C4S4}. Analysis was also performed for one variant where all cysteines were mutated into serines (IDO_{C0S8}) and another variant where all cysteines were mutated into alanines (IDO_{C0A8}). Residue distance between r85 and r129 was measured using Mol* Viewer (RCSB PDB) (40).

Galectin 3 binding affinity

Affinity of IDO_{C4S4}-Gal3 for lactose was determined using affinity chromatography in an AKTA Pure chromatography system (GE Life Sciences) equipped with consumer-packable glass column (GE Life Sciences) packed with α -lactose agarose affinity resin (Sigma-Aldrich). Proteins were eluted with a linear gradient of β -lactose (Sigma-Aldrich) in phosphate buffer.

Secondary structure

Protein secondary structure characteristics were measured using Fourier-transform infrared (FT-IR) spectroscopy (PerkinElmer, USA) and circular dichroism (CD). CD was recorded on a Chirascan™-plus qCD (Applied Phosphysics) with a quartz cuvette of path length 1 mm from wavelengths between 190 and 260 nm with 2 nm intervals. Each sample contained purified protein at $\sim 0.1 \text{ mg} \cdot \text{mL}^{-1}$ and both sample and baseline contained 10 mM phosphate, pH 7.4, and 140 mM KF. Samples were scanned 5 times with the average spectra reported. For FT-IR, wild-type IDO_{C8S0}, IDO_{C5S3}, and IDO_{C4S4} in distilled water were lyophilized from frozen. Samples were transferred onto the attenuated total reflectance (ATR) stage and then powder samples were compressed by pressure device to give uniform contact on the ATR crystal. The absorbance spectrum was measured over the range of 900–4000 cm^{-1} . The baseline of each spectrum was corrected using the Baseline Correction function within the PerkinElmer Spectrum software. Absorbance at 1650 cm^{-1} represents amide I band, while absorbance at 1550 cm^{-1} corresponds to the amide II band. Secondary structure comparisons were made from the peak shape and intensity of amide I and II bands.

Imiquimod-Induced Psoriasis

All studies were conducted with the approval of the University of Florida Internal Animal Care and Use Committee, in compliance with the United States Public Health Service policy on Humane Care and Use of Laboratory Animals. An inflammatory mouse model, imiquimod-induced psoriasis (7,41), was used to confirm therapeutic efficacy of IDO-Gal3 mutants. After shaving and removal of remaining hair with depilatory cream, 62.5 μg of 5% imiquimod cream (Patterson Veterinary Supply, cat. num. 07-893-7787), a potent inflammatory agent, was applied to the backs of female C57/BL6J mice (8 weeks old, Jackson labs, PBS: $n = 8$, all others: $n = 4$). Mice were clinically observed and scored daily using a modified Psoriasis Area and Severity Index (PASI) score to determine disease severity. Erythema (redness), scaling, and thickening were scored independently and assigned a score between 0 to 4: 0, none, 1: slight, 2: moderate, 3: marked, 4: very marked. The cumulative score was reported as a measure of the severity of inflammation (scale 0-12). On the first day of clinical score emergence (day 3), five 10 μg doses of IDO_{C4S4}-Gal3, IDO-Gal3, or an equivalent volume of PBS were injected subcutaneously and evenly distributed across the back. Application of imiquimod cream and clinical scoring was performed every day for a duration of 10 d. Mean clinical scores were compared using a one-way ANOVA and Dunnett's multiple comparisons test. Area under the curve was calculated for each animal, and compared using an unpaired t-test. Initial rate of change of scores was measured between the baseline score to plateau for each animal, and compared using an unpaired t-test. All statistics were performed using Graphpad Prism.



Results and Discussion

Cysteine to serine IDO mutants are enzymatically active

We designed two different IDO mutants, one where the cysteines located at residues 112, 159, 206, and 308 were substituted for serines, “IDO_{C4S4}”, and a second at residues 112, 159, and 308, “IDO_{C5S3}” (**Figure 1A**). Proteins corresponding to the predicted molecular weights of IDO_{C4S4} and IDO_{C5S3} were recovered in good yield and purity from microbial hosts (**Figure 1B**). Soret bands ($\lambda = 405\text{--}425\text{ nm}$), which are used to identify the heme unit of IDO (42), had similar maxima for WT IDO, IDO_{C4S4} and IDO_{C5S3} (**Figure 1C**). Wild-type IDO (“WT IDO_{C8S0}”) had a higher Soret band/protein ($\lambda = 405/280\text{ nm}$) peak ratio than that of IDO_{C4S4} and IDO_{C5S3}, suggesting that there may be more heme bound to WT IDO. Both IDO mutant forms were enzymatically active (**Figure 1D**). There were no differences in K_M for either mutant relative to WT IDO; however, IDO_{C5S3} had significantly slower V_{\max} value than WT IDO_{C8S0} and IDO_{C4S4}. This slower V_{\max} and weaker Soret band of IDO_{C5S3} are correlative, as heme binding to oxygen is required for the dioxygenase reaction of tryptophan^{17,25}.

In silico analysis and *in vitro* secondary structure characterization display a high degree of similarity between WT IDO and cysteine-based mutants

Computational models predicted that the Cys-Ser mutations in IDO_{C5S3} and IDO_{C4S4} would not significantly alter secondary structures compared to WT IDO. Composition of predicted secondary structure components showed no significant changes (**Figure 2A**), and three-dimensional structural predictions between WT IDO and IDO mutants had a high degree of similarity (**Figure 2B**). Likewise, CD and FT-IR measurements showed that the secondary structures of IDO_{C5S3} and IDO_{C4S4} were highly similar to that of WT IDO. The CD spectra of all three proteins were characterized by minima at 208 and 222 nm, along with a maxima at 192 nm (**Figure 2C**), consistent with a protein that is predominantly folded into alpha-helices. Additionally, all three proteins demonstrated a prominent peak at $1645\text{--}1655\text{ cm}^{-1}$ in FT-IR spectra, indicating a structure predominated by alpha-helical coiled-coils (**Figure 2D**), matching characterizations of IDO in the literature (17,43). Of note, IDO_{C5S3} displayed a slight blue shift in the maxima of the primary amide band to 1652.5 cm^{-1} (**Figure 2E**), which suggests a subtle shift in secondary structure (44), and which correlates to the slower V_{\max} seen in this mutant.

Cysteine to Serine mutants improve IDO thermal stability at physiological and reduced temperatures

To assess the effect of the Cys-Ser mutants on thermal stability of IDO, we measured the enzymatic function of WT IDO and the two mutants after warm (37 °C), room temperature (25 °C), and cold (4 °C) storage. Cys-Ser mutants demonstrated higher enzymatic activity over time when compared to WT IDO (**Figure 3A**). At physiological temperatures, IDO_{C4S4} extended enzymatic half-life by ~50% as compared to WT IDO_{C8S0}, whereas IDO_{C5S3} only extended stability by ~20% (**Figure 3B**). At room temperature, IDO_{C4S4} increased half-life by ~200% compared to WT IDO_{C8S0}, while IDO_{C5S3} only improved the half-life on the order of hours rather than days (**Figure 3B**). Cold storage showed the best improvement in enzymatic stability, as both mutant forms increased the enzymatic half-life by 200% (~1 week increase) as compared to WT (**Figure 3B**). Consistent with this result, cysteine point mutations have been previously reported to improve cold storage and thermostability (45,46), suggested to be due to slowed or absent cysteine oxidation (47). Such mutations, however, would not be expected to affect the



susceptibility of the heme to oxidative degradation, as has been shown for IDO and other proteins (8,48).

Cysteine to Serine IDO mutations improve therapeutic efficacy in imiquimod-induced psoriasis

We created a fusion of IDO_{C4S4} and galectin 3 (Gal3) (**Figure 4A**) based on our prior work showing that IDO-Gal3 is effective for treating local inflammation in various diseases (7,49). IDO_{C5S3} was excluded from these studies based on its diminished V_{\max} and weaker thermal stability when compared to IDO_{C4S4}. IDO_{C4S4}-Gal3 was expressed and recovered in high yield and purity (**Figure 4B**). Tryptophan catabolism was comparable between IDO_{C4S4} and IDO_{C4S4}-Gal3 (**Figure 4C**). The Gal3 domain endowed IDO_{C4S4}-Gal3 with binding affinity for immobilized lactose that IDO_{C4S4} lacked, as expected (**Figure 4D**).

To test the *in vivo* immunomodulatory capabilities of our IDO Cys-Ser mutant, we used the IMQ-induced psoriasis mouse model, as previously described (7). Mice were treated one time with 50 μ g subcutaneous injections of IDO-Gal3 or IDO_{C4S4}-Gal3, or with an equivalent volume of PBS vehicle control at the first sign of clinical symptoms (erythema, skin thickening, and skin scaling) (**Figure 4E**). IDO_{C4S4}-Gal3 blunted disease progression of psoriasis (**Figure 4F**). Treatment with the mutant led to significantly lower area under the curve for clinical scores relative to vehicle control (**Figure 4G**). Treatment with the mutant also delayed peak of disease and slowed rate of inflammation compared to the existing IDO-Gal3 fusion (**Figure 4H**). This improved effectiveness of the IDO_{C4S4} mutant corresponded with its increased enzymatic stability and faster V_{\max} .

Models predict the influence of cysteine mutations to IDO structure

Modeling of crystal structures predicted that Cys-Ala mutations would change the inter-residue distance between residue 85 and residue 129, which surrounds the enzymatic pocket (27). This was suggested to change substrate binding through altered hydrophobic interactions, resulting in a loss of enzymatic activity. Modeling of IDO using AlphaFold v3 predicted that total protein architecture, as measured with RMSD and TM, was not altered in the IDO_{C4S4} and IDO_{C5S3} mutants (**Figure 5B**), whereas it was altered in the Cys-Ala mutants reported previously (**Figure 5A**). Likewise, AlphaFold v3 models predicted that inter-residue distances would increase when all Cys were mutated to Ala, IDO_{C0A8}, while the selective mutations of IDO_{C5S3} and IDO_{C4S4} were not predicted to increase inter-residue distances (**Figure 5B**). Notably, mutating all IDO Cys residues to Ser (IDO_{C0S8}) was predicted to significantly increase inter-residue distances, which we expected would lead to reduced activity. Indeed, the IDO_{C0S8} mutant was recovered in poor yield and showed less than 1% activity when compared to IDO_{C8S0}, IDO_{C4S4}, and IDO_{C5S3} (**Figure 5B**). However, even when inter-residue distances were predicted to be similar, as with IDO_{C5S3} and IDO_{C4S4}, inserting Ser residues into IDO could have some effect on enzyme activity, as suggested by the slower V_{\max} for IDO_{C5S3} than for wild-type and IDO_{C4S4}, despite IDO_{C5S3} sharing C206 with wild-type, whereas IDO_{C4S4} did not. (**Figure 1D**). Collectively, these data suggest that while computational models can be used to predict the tolerability of IDO structure to mutations, the impact on enzymatic activity is complex, depending on both the type and placement of the residues, and so must be arrived at empirically.

Conclusions



The IDO_{C4S4} mutant demonstrated marked improvement in thermal stability and reaction velocity, which provided for a more effective protein therapeutic in the context of psoriasis. Improving reaction velocity and thermal stability of enzymes is often difficult, as protein properties *in vitro* versus *in vivo* can vary due to many different factors (50,51). These improvements were made by mutating surface accessible cysteines to chemically-similar serines, while maintaining cysteines thought to be buried within the fold of IDO. In contrast, prior work using Cys-Ala mutations led to significant decreases in IDO activity (27). Collectively, these data reinforce the idea that amino acid choice and site selection are critical for engineering improved mutant enzymes.

Author contributions

J.A.S, A.W., B.G.K., and G.A.H. conceived of this study. J.A.S, A.W., and A.S. conducted protein production and enzymatic activity assessment. R.A.C and J.P. conducted secondary structure characterization. J.A.S. performed computational modeling and animal experiments. J.A.S. performed data analysis and wrote the draft of the manuscript. J.A.S., B.G.K., and G.A.H. finalized the manuscript. All authors approved the submitted version of this paper. Artificial intelligence, such as ChatGPT, did not write the manuscript or generate figures outside of AlphaFold v3 predictions, which have been disclosed.

Conflicts of interest

There are no conflicts to declare.

Data availability

Amino acid sequences can be found in the supplement.

Acknowledgements

We would like to thank Dr. Brandon D. Wiles for his assistance with mathematical modeling. B.G.K. and G.A.H. disclose support for the research described in this study from the National Institutes of Health (R01 DE027301). B.G.K. discloses support from the National Institutes of Health (R01 DK091658, R01 DK098589, and R01 AI133623). G.A.H. discloses support from the National Institutes of Health (R03 EB019684 and R35 GM133697) and the National Science Foundation (DMR-1455201).



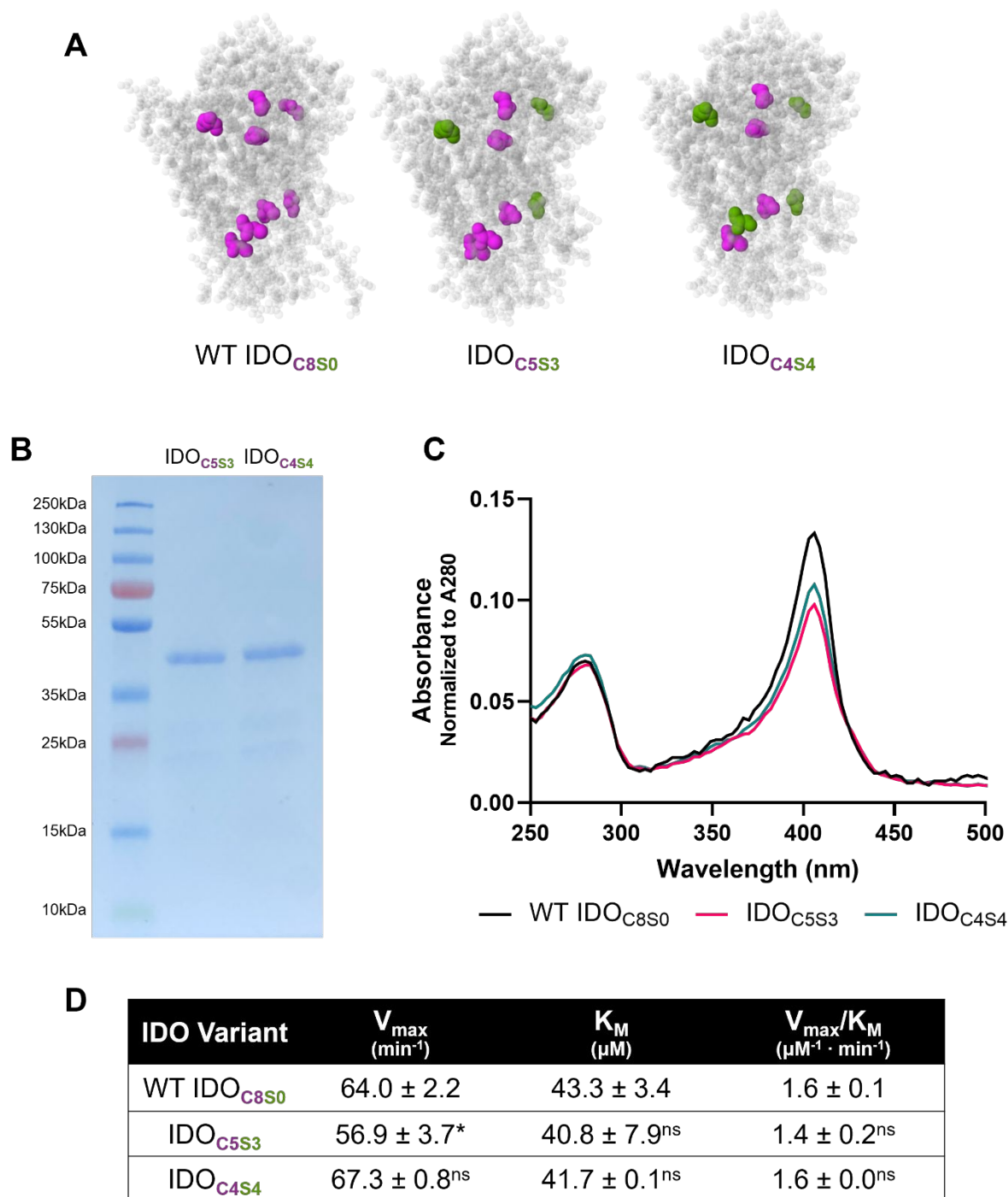


Figure 1. IDO Cys-Ser Mutants. (A) Predicted IDO crystal structures highlighting the location of Cys residues in each IDO variant. Cysteines are highlighted in pink while cysteine to serine point mutations are highlighted in green. (B) SDS-PAGE gel of IDO_{C5S3} and IDO_{C4S4} showing a pure product after recombinant expression. (C) Absorbance spectra of WT IDO_{C8S0}, IDO_{C5S3}, and IDO_{C4S4}, with Soret peak around 405 nm. (D) Enzymatic parameters of WT and mutant IDO, compared between mutant and WT. *: P < 0.05, ns: no significance

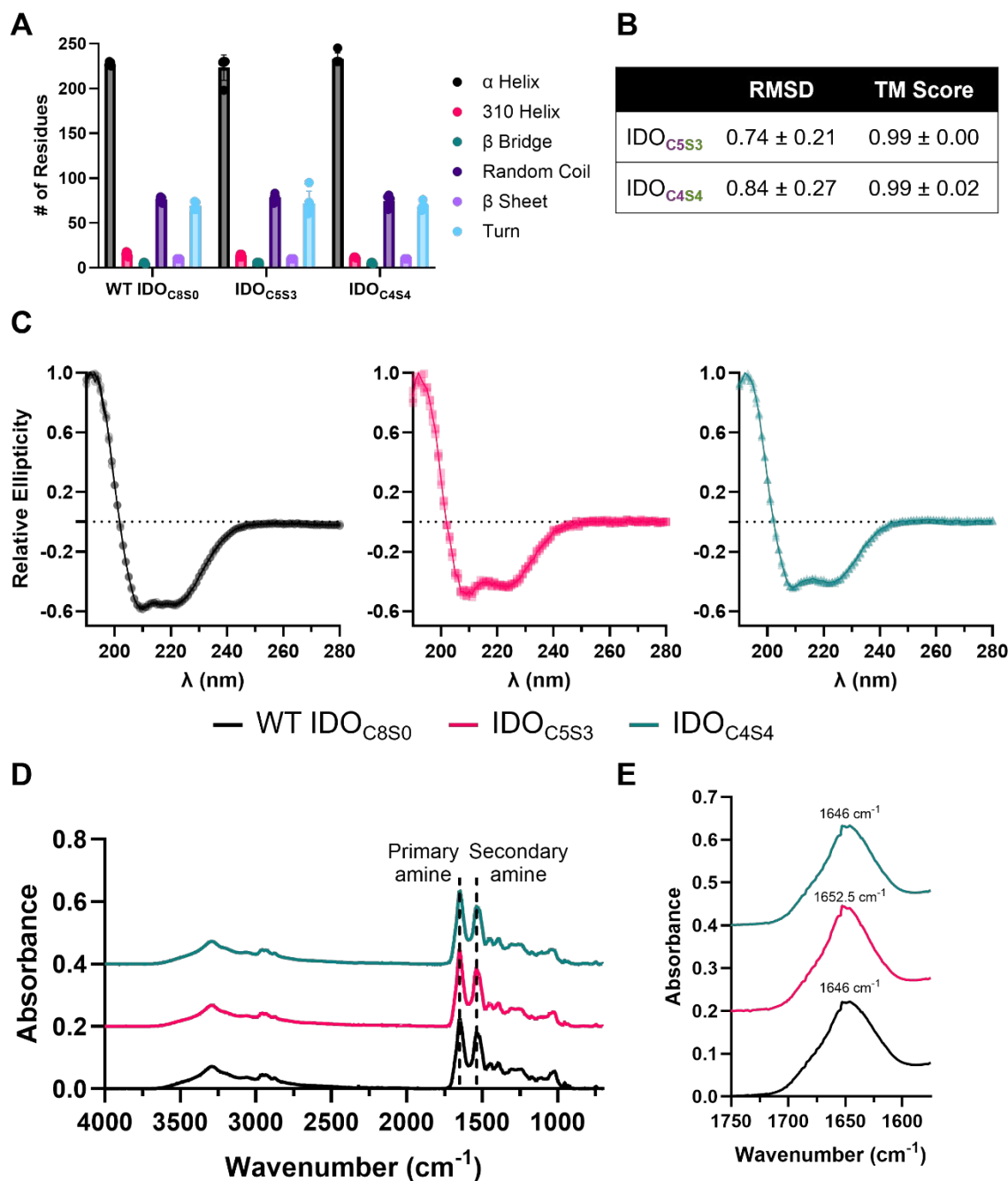
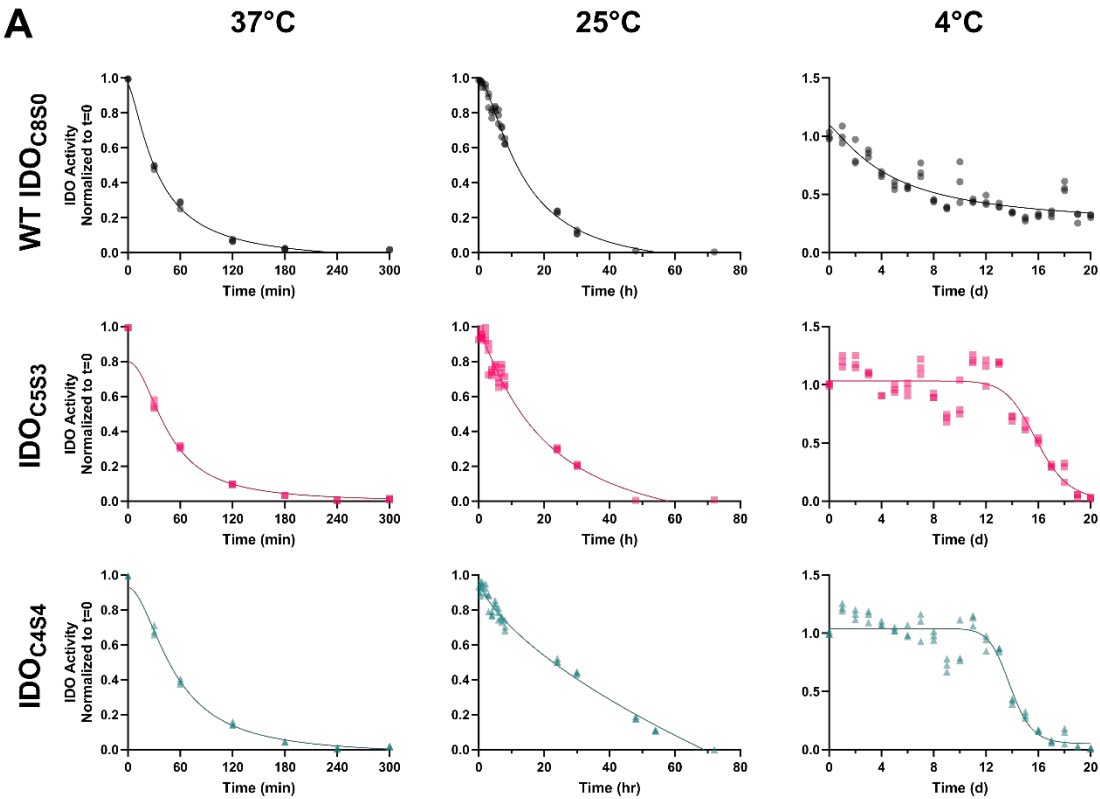


Figure 2. IDO mutants have similar *in silico* predicted and *in vitro* secondary structures. (A) Secondary structure composition comparison and (B) pairwise structural alignment comparison between AlphaFold predictions of WT IDO and IDO Cys-Ser mutants. (C) Circular Dichroism spectra of IDO proteins over the range $\lambda=180$ to $\lambda=280$ nm at 20 °C. (D) Fourier transform infrared spectroscopy (FT-IR) absorbance spectra of IDO and Cys-Ser mutants. Dashed lines at indicate primary and secondary amines. (E) Inset of FT-IR trace, showing primary amine.





B

IDO Variant	Half Life – 37°C	Half Life – 25°C	Half Life – 4°C
WT IDO _{C8S0}	29.9 ± 1.2 min	11.6 ± 0.4 h	8.8 ± 0.6 d
IDO _{C5S3}	35.3 ± 2.1 min*	13.1 ± 0.6 h ^{ns}	16.2 ± 0.1 d****
IDO _{C4S4}	47.1 ± 1.9 min****	22.5 ± 0.7 h****	14.6 ± 0.1 d****

Figure 3. Cys-Ser IDO mutants increase stability of IDO. (A) WT vs IDO_{C5S3} vs IDO_{C4S4} normalized enzymatic activity over time after storage at 37 °C, 25 °C, and 4 °C. (B) Mutant IDO activity half-life also increases for all temperatures, as compared to WT IDO_{C8S0}. *: P < 0.05, ****: P < 0.0001



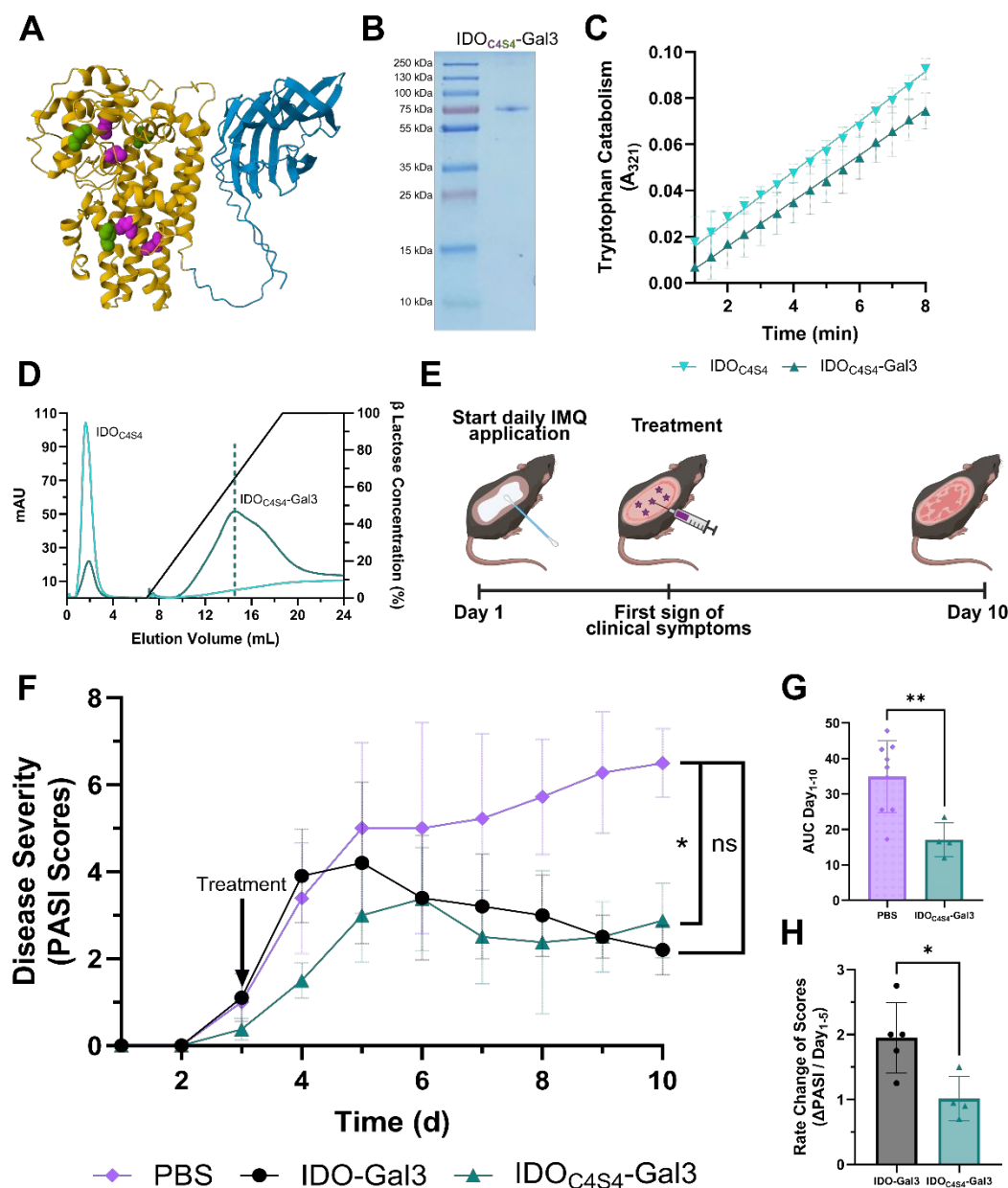


Figure 4. Anchored Cys-Ser IDO mutant improves therapeutic efficacy. (A) Schematic of IDO_{C4S4}-Gal3, with the IDO arm shown in yellow and the Gal3 arm shown in blue. Cysteines are highlighted in pink while cysteine to serine point mutations are highlighted in green. (B) SDS-PAGE gel of IDO_{C4S4}-Gal3, showing a pure product after recovery. (C) Tryptophan catabolism of IDO_{C4S4} and IDO_{C4S4}-Gal3, as shown by absorbance at 321 nm over time. (D) Lactose binding affinity of IDO_{C4S4} and IDO_{C4S4}-Gal3, showing preserved Galectin 3 functionality in the fusion mutant. (E) Timeline of IMQ-induced psoriasis mouse model. Subcutaneous injection sites are depicted as purple stars. (F) Mutant IDO_{C4S4}-Gal3 reduces clinical scores in psoriatic mouse model as compared to PBS treatment, while IDO-Gal3 does not achieve statistical significance of cumulative clinical scores. (G) Area under the curve of clinical scoring is significantly reduced in IDO_{C4S4}-Gal3 as compared to PBS. (H) IDO_{C4S4}-Gal3 blunts peak of disease and slows rate of inflammation as compared to IDO-Gal3. *: P < 0.05, **: P < 0.005, ns: no significance.



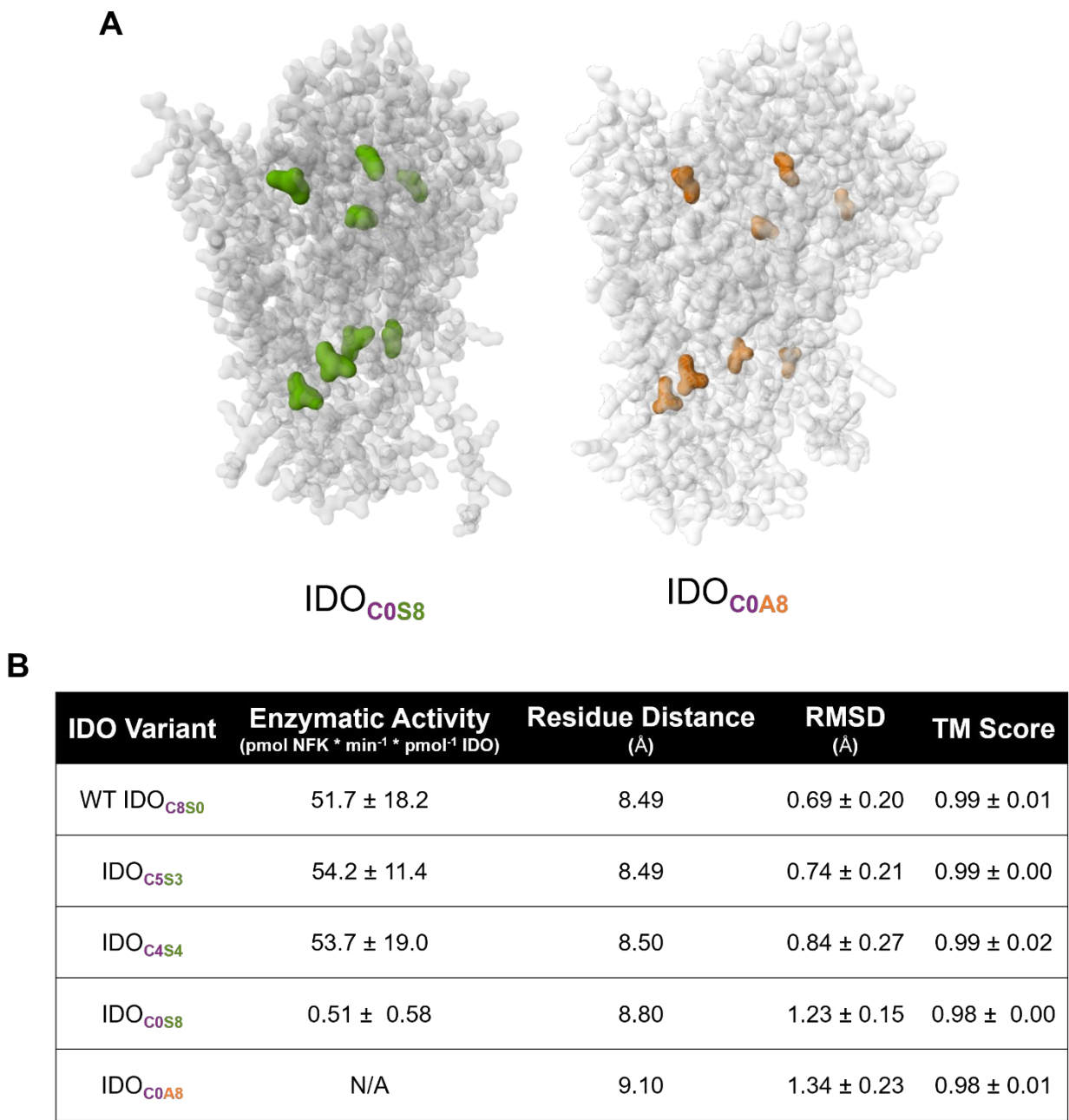


Figure 5. Mutation of cysteines to serines preserves residue distance surrounding enzymatic site. (A) Predicted crystal structures of all Cys-Ser (left) and all Cys-Ala (right) mutations of IDO. Cysteine to serine point mutations are highlighted in green and cysteine to alanine point mutations are highlighted in orange (B) Activity, predicted distance between site 85 and site 129, and pairwise structural alignment comparison for all mutations.





References

1. Yeung AWS, Terentis AC, King NJC, Thomas SR. Role of indoleamine 2,3-dioxygenase in health and disease. *Clin Sci*. 2015 Oct;129(7):601–72.
2. Zhang Y, Jalili RB, Kilani RT, Elizei SS, Farrokhi A, Khosravi-Maharlooei M, et al. IDO-Expressing Fibroblasts Protect Islet Beta Cells From Immunological Attack and Reverse Hyperglycemia in Non-Obese Diabetic Mice. *J Cell Physiol*. 2016 Sept;231(9):1964–73.
3. Jalili RB, Zhang Y, Hosseini-Tabatabaei A, Kilani RT, Khosravi Maharlooei M, Li Y, et al. Fibroblast Cell-Based Therapy for Experimental Autoimmune Diabetes. *PLoS ONE*. 2016 Jan 14;11(1):e0146970.
4. Elizei SS, Pakyari M, Ghoreishi M, Kilani R, Mahmoudi S, Ghahary A. IDO-expressing Fibroblasts Suppress the Development of Imiquimod-induced Psoriasis-like Dermatitis. *Cell Transplant*. 2018 Mar;27(3):557–70.
5. Kenney LL, Chiu RSY, Dutra MN, Wactor A, Honan C, Shelerud L, et al. mRNA-delivery of IDO1 suppresses T cell-mediated autoimmunity. *Cell Rep Med*. 2024 Sept 17;5(9):101717.
6. Bracho-Sanchez E, Hassanzadeh A, Brusko MA, Wallet MA, Keselowsky BG. Dendritic Cells Treated with Exogenous Indoleamine 2,3-Dioxygenase Maintain an Immature Phenotype and Suppress Antigen-specific T cell Proliferation. *J Immunol Regen Med* [Internet]. 2019 Sept [cited 2022 Feb 1];5. Available from: <https://linkinghub.elsevier.com/retrieve/pii/S2468498818300465>
7. Bracho-Sanchez E, Rocha FG, Bedingfield SK, Partain BD, Macias SL, Brusko MA, et al. Suppression of local inflammation via galectin-anchored indoleamine 2,3-dioxygenase. *Nat Biomed Eng*. 2023 Sept;7(9):1156–69.
8. Freewan M, Rees MD, Plaza TSS, Glaros E, Lim YJ, Wang XS, et al. Human indoleamine 2,3-dioxygenase is a catalyst of physiological heme peroxidase reactions: implications for the inhibition of dioxygenase activity by hydrogen peroxide. *J Biol Chem*. 2013 Jan 18;288(3):1548–67.
9. Ohtaki H, Ito H, Ando K, Ishikawa T, Hoshi M, Tanaka R, et al. Interaction between LPS-induced NO production and IDO activity in mouse peritoneal cells in the presence of activated Valpha14 NKT cells. *Biochem Biophys Res Commun*. 2009 Nov 13;389(2):229–34.
10. Alberati-Giani D, Malherbe P, Ricciardi-Castagnoli P, Köhler C, Denis-Donini S, Cesura AM. Differential regulation of indoleamine 2,3-dioxygenase expression by nitric oxide and inflammatory mediators in IFN-gamma-activated murine macrophages and microglial cells. *J Immunol*. 1997 July;159(1):419–26.
11. Hücke C, MacKenzie CR, Adjogble KDZ, Takikawa O, Däubener W. Nitric oxide-mediated regulation of gamma interferon-induced bacteriostasis: inhibition and degradation of human indoleamine 2,3-dioxygenase. *Infect Immun*. 2004 May;72(5):2723–30.
12. Hill M, Zagani R, Voisine C, Usal C, Anegón I. Nitric oxide and indoleamine 2,3-dioxygenase mediate CTLA4Ig-induced survival in heart allografts in rats. *Transplantation*. 2007 Oct 27;84(8):1060–3.



13. Fujigaki H, Saito K, Lin F, Fujigaki S, Takahashi K, Martin BM, et al. Nitration and inactivation of IDO by peroxynitrite. *J Immunol.* 2006;176(1):372–9.
14. Lugrin J, Rosenblatt-Velin N, Parapanov R, Liaudet L. The role of oxidative stress during inflammatory processes. *Biol Chem.* 2014 Feb;395(2):203–30.
15. Manoharan RR, Prasad A, Pospíšil P, Kzhyshkowska J. ROS signaling in innate immunity via oxidative protein modifications. *Front Immunol.* 2024 Mar 7;15:1359600.
16. Poljak A, Grant R, Austin CJD, Jamie JF, Willows RD, Takikawa O, et al. Inhibition of indoleamine 2,3 dioxygenase activity by H₂O₂. *Arch Biochem Biophys.* 2006 June;450(1):9–19.
17. Sugimoto H, Oda S ichiro, Otsuki T, Hino T, Yoshida T, Shiro Y. Crystal structure of human indoleamine 2,3-dioxygenase: catalytic mechanism of O₂ incorporation by a heme-containing dioxygenase. *Proc Natl Acad Sci USA.* 2006 Feb 21;103(8):2611–6.
18. Cogley JN. 50 shades of oxidative stress: A state-specific cysteine redox pattern hypothesis. *Redox Biol.* 2023 Nov;67:102936.
19. Perry LJ, Wetzel R. The role of cysteine oxidation in the thermal inactivation of T4 lysozyme. *Protein Eng.* 1987;1(2):101–5.
20. Garrido Ruiz D, Sandoval-Perez A, Rangarajan AV, Gunderson EL, Jacobson MP. Cysteine oxidation in proteins: structure, biophysics, and simulation. *Biochemistry.* 2022 Oct 18;61(20):2165–76.
21. Fomenko DE, Marino SM, Gladyshev VN. Functional diversity of cysteine residues in proteins and unique features of catalytic redox-active cysteines in thiol oxidoreductases. *Mol Cells.* 2008 Sept 30;26(3):228–35.
22. Klomsiri C, Karplus PA, Poole LB. Cysteine-based redox switches in enzymes. *Antioxid Redox Signal.* 2011 Mar 15;14(6):1065–77.
23. Moon KH, Hood BL, Mukhopadhyay P, Rajesh M, Abdelmegeed MA, Kwon YI, et al. Oxidative inactivation of key mitochondrial proteins leads to dysfunction and injury in hepatic ischemia reperfusion. *Gastroenterology.* 2008 Oct;135(4):1344–57.
24. Suh SK, Hood BL, Kim BJ, Conrads TP, Veenstra TD, Song BJ. Identification of oxidized mitochondrial proteins in alcohol-exposed human hepatoma cells and mouse liver. *Proteomics.* 2004 Nov;4(11):3401–12.
25. Klaessens S, Stroobant V, De Plaen E, Van den Eynde BJ. Systemic tryptophan homeostasis. *Front Mol Biosci.* 2022 Sept 14;9:897929.
26. Terentis AC, Freewan M, Sempértegui Plaza TS, Raftery MJ, Stocker R, Thomas SR. The selenazal drug ebselen potently inhibits indoleamine 2,3-dioxygenase by targeting enzyme cysteine residues. *Biochemistry.* 2010 Jan 26;49(3):591–600.



27. Austin CJD, Kosim-Satyaputra P, Smith JR, Willows RD, Jamie JF. Mutation of cysteine residues alters the heme-binding pocket of indoleamine 2,3-dioxygenase-1. *Biochem Biophys Res Commun*. 2013;
28. Bywater RP. Why twenty amino acid residue types suffice(d) to support all living systems. *PLoS ONE*. 2018 Oct 15;13(10):e0204883.
29. Ahmed MH, Catalano C, Portillo SC, Safo MK, Neel Scarsdale J, Kellogg GE. 3D interaction homology: The hydrophobic interaction environments of even alanine are diverse and provide novel structural insight. *J Struct Biol*. 2019 Aug;207(2):183–98.
30. Gisdon FJ, Bombarda E, Ullmann GM. Serine and Cysteine Peptidases: So Similar, Yet Different. How the Active-Site Electrostatics Facilitates Different Reaction Mechanisms. *J Phys Chem B*. 2022 June 9;126(22):4035–48.
31. Catalano C, Al Mughram MH, Guo Y, Kellogg GE. 3D interaction homology: Hydrophobic interaction environments of serine and cysteine are strikingly different and their roles adapt in membrane proteins. *Current Research in Structural Biology*. 2021 Oct;3:239–56.
32. Fettis MM, Hudalla GA. Engineering Reactive Oxygen Species-Resistant Galectin-1 Dimers with Enhanced Lectin Activity. *Bioconj Chem*. 2018 July 18;29(7):2489–96.
33. Saetang J, Roongsawang N, Sangkhathat S, Voravuthikunchai SP, Sangkaew N, Prompat N, et al. Surface cysteine to serine substitutions in IL-18 reduce aggregation and enhance activity. *PeerJ*. 2022 July 5;10:e13626.
34. Pavlin M, Qasem Z, Sameach H, Gevorgyan-Airapetov L, Ritacco I, Ruthstein S, et al. Unraveling the Impact of Cysteine-to-Serine Mutations on the Structural and Functional Properties of Cu(I)-Binding Proteins. *Int J Mol Sci [Internet]*. 2019 July 14 [cited 2024 Feb 28];20(14). Available from: <http://dx.doi.org/10.3390/ijms20143462>
35. eLabProtocols - ZYM-5052 medium for auto-induction [Internet]. [cited 2024 Mar 7]. Available from: <https://www.elabprotocols.com/protocols/#!/protocol=38033>
36. Abramson J, Adler J, Dunger J, Evans R, Green T, Pritzel A, et al. Accurate structure prediction of biomolecular interactions with AlphaFold 3. *Nature*. 2024 June;630(8016):493–500.
37. Ye Y, Godzik A. Flexible structure alignment by chaining aligned fragment pairs allowing twists. *Bioinformatics*. 2003 Oct;19 Suppl 2:ii246-55.
38. Li Z, Jaroszewski L, Iyer M, Sedova M, Godzik A. FATCAT 2.0: towards a better understanding of the structural diversity of proteins. *Nucleic Acids Res*. 2020 July 2;48(W1):W60–4.
39. Heinig M, Frishman D. STRIDE: a web server for secondary structure assignment from known atomic coordinates of proteins. *Nucleic Acids Res*. 2004 July;32(Web Server issue):W500-2.



40. Sehna D, Bittrich S, Deshpande M, Svobodová R, Berka K, Bazgier V, et al. Mol* Viewer: modern web app for 3D visualization and analysis of large biomolecular structures. *Nucleic Acids Res.* 2021 July 2;49(W1):W431–7.
41. van der Fits L, Mourits S, Voerman JSA, Kant M, Boon L, Laman JD, et al. Imiquimod-induced psoriasis-like skin inflammation in mice is mediated via the IL-23/IL-17 axis. *J Immunol.* 2009 May;182(9):5836–45.
42. Huber WJ, Backes WL. Quantitation of heme oxygenase 1: heme titration increases yield of purified protein. *Anal Biochem.* 2008 Feb;373(1):167–9.
43. Röhrig UF, Michielin O, Zoete V. Structure and Plasticity of Indoleamine 2,3-Dioxygenase 1 (IDO1). *J Med Chem.* 2021 Dec 23;64(24):17690–705.
44. Chiang KY, Matsumura F, Yu CC, Qi D, Nagata Y, Bonn M, et al. True Origin of Amide I Shifts Observed in Protein Spectra Obtained with Sum Frequency Generation Spectroscopy. *J Phys Chem Lett.* 2023 June;14(21):4949–54.
45. Seid CA, Jones KM, Pollet J, Keegan B, Hudspeth E, Hammond M, et al. Cysteine mutagenesis improves the production without abrogating antigenicity of a recombinant protein vaccine candidate for human chagas disease. *Hum Vaccin Immunother.* 2017 Mar 4;13(3):621–33.
46. Lee J, Blaber M. The interaction between thermodynamic stability and buried free cysteines in regulating the functional half-life of fibroblast growth factor-1. *J Mol Biol.* 2009 Oct 16;393(1):113–27.
47. Nakaniwa T, Fukada H, Inoue T, Gouda M, Nakai R, Kirii Y, et al. Seven cysteine-deficient mutants depict the interplay between thermal and chemical stabilities of individual cysteine residues in mitogen-activated protein kinase c-Jun N-terminal kinase 1. *Biochemistry.* 2012 Oct 23;51(42):8410–21.
48. Di Rocco G, Bernini F, Battistuzzi G, Ranieri A, Bortolotti CA, Borsari M, et al. Hydrogen peroxide induces heme degradation and protein aggregation in human neuroglobin: roles of the disulfide bridge and hydrogen-bonding in the distal heme cavity. *FEBS J.* 2023;290(1):148–61.
49. Farhadi SA, Bracho-Sanchez E, Fettis MM, Seroski DT, Freeman SL, Restuccia A, et al. Locally anchoring enzymes to tissues via extracellular glycan recognition. *Nat Commun.* 2018 Nov 22;9(1):4943.
50. Hingorani KS, Gierasch LM. Comparing protein folding in vitro and in vivo: foldability meets the fitness challenge. *Curr Opin Struct Biol.* 2014 Feb;24:81–90.
51. Feng R, Gruebele M, Davis CM. Quantifying protein dynamics and stability in a living organism. *Nat Commun.* 2019 Mar 12;10(1):1179.



Data availability

Amino acid sequences can be found in the supplement.

